DISCLAIMER

This book was prepared as an account of work sponsored by an agency of the United States Government. Neither the United States Government nor any agency thereof, nor any of their employees, makes any warranty, express or implied, or assumes any legal liability or responsibility for the accuracy, completeness, or usefulness of any information, apparatus, product, or process disclosed, or represents that its use would not infringe privately owned rights. Reference herein to any specific commercial product, process, or service by trade name, trademark, manufacturer, or otherwise, does not necessarily constitute or imply its endorsement, recommendation, or favoring by the United States Government or any agency thereof. The views and opinions of authors expressed herein do not necessarily state or reflect those of the United States Government or any agency thereof.

PROPERTIES OF NUCLEI AT VERY HIGH SPIN

F. S. Stephens

Lawrence Berkeley Laboratory
University of California
Berkeley, CA 94720

Abstract: Nuclear structure at very high spins involves an interplay between collective (often rotational) and noncollective (individual particle alignment) behavior. The new techniques for studying γ-ray energy correlations promise to give detailed information about both of these aspects of nuclear behavior up to the very highest spins that can be populated.

1. Introduction

Our understanding of the structure of high-spin states has developed rapidly in the last few years. A rather satisfying perspective is now emerging which I will try to convey to you. I will discuss γ-ray studies because at present they give much the most detailed information about nuclear structure at these spin values.

A first question has to do with the amount of angular momentum that one can get into γ-ray cascades. By far the best method presently known to produce high-spin states is through heavy-ion fusion reactions. The maximum angular momentum that results in γ emission following such reactions is shown in fig. 1. Above and to the right of the curve in fig. 1, the angular momentum is lost through fission; whereas above and to the left, it is removed by particle (largely α) evaporation. Below the line γ emission

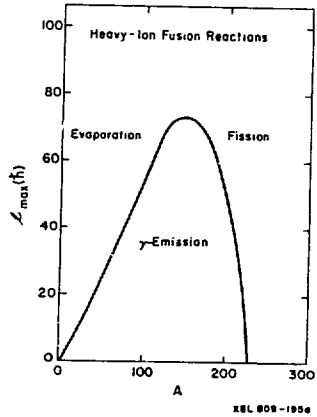

Fig. 1. The line indicates the limiting angular momentum for a nucleus (of mass A) between γ-ray emission (below) and either fission (above, right) or particle evaporation (above, left).

DISTRIBUTION OF THIS DOCUMENT IS UNLIMITED

dominates and deexcites the nucleus to its ground state. It is apparent that the highest angular momentum that decays through γ emission is about 70 ħ for masses around 150. If these nuclei could be produced cold, only about 15 to 20 ħ more could be retained. Thus we can study most of the possible range. In this talk I will concentrate on this mass region--the light rare-earth nuclei.

To understand the structure of nuclei at such spins I want to begin by considering a classical rigid rotor. It is not clear that nuclei behave this way, though at high spins, where the pairing correlations are quenched, most people believe this is approximately true. Two limiting models for nuclear behavior suggest that it is reasonable[1]). The moment of inertia of a rigid ellipsoid (having constant volume) compared with that of a rigid sphere is shown in fig. 2 as a function of shape (γ) for two deformation

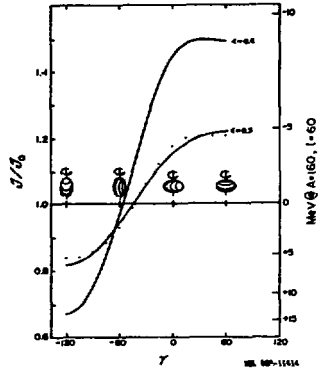

Fig. 2. Ratio of the moment of inertia of a rigid ellipsoid to that of a rigid sphere vs the shape parameter γ for two values of the deformation ε = 0.3 and ε = 0.6. The right-hand scale gives the difference in rotational energy in MeV for a nucleus with A = 160 and I = 60. The dots give the differences in total liquid-drop energy (rotation + surface + Coulomb) for the nucleus.

values. The value ε ≈ 0.3 corresponds roughly to that found in deformed rare-earth nuclei, whereas ε ≈ 0.6 corresponds to an axis ratio of about 2:1--the largest that one could hope to see in these (or probably any) nuclei. It is clear in fig. 2 that there is a favored region of large moments of inertia, extending from an oblate shape rotating about its symmetry axis (γ = 60°) to a prolate shape rotating about a perpendicular axis (γ = 0°). To see just how significant this favoring is, I have put an energy scale on the right side of fig. 2 for the case of mass 160 and spin 60 ħ. These shapes are seen to be favored by about 10 MeV over the others. Since the average shell effects are only around 3 MeV, these moment-of-inertia effects should dominate at high spins and restrict the nuclei to the above shape region. It is interesting that the shape dependence of the surface and Coulomb energy terms in the liquid drop model is small, and the full LDM energy, given by the dots on fig. 2, is remarkably near to that obtained from the moments of inertia alone--simply geometry.

There is a further aspect of these shapes that is important. The rotation of a nucleus about an axis perpendicular to the symmetry is a collective rotation with smooth bands and strongly enhanced E2 transitions connecting the levels. There are many beautiful examples of such rotors in the region around mass 160. On the other hand a quantal system like the nucleus cannot rotate around a symmetry axis. This degree of freedom is contained in the single-particle motions. Thus a nucleus of $\gamma = 60^0$ builds up its angular momentum by aligning that of one or more individual nucleons with the symmetry axis. This is completely noncollective and is much like the case of spherical closed-shell nuclei. It seems that around mass 150 some oblate nuclei exist[2,3], with such noncollective states running up to around 40 ħ. I will try to convince you in this talk that nuclei at the highest spins like to be between these limits ($\gamma = 0^0$ and 60^0), displaying some collective and some noncollective properties.

2. Backbending region

I will begin at reasonably low spins--around 20 ħ. A plot of energy versus spin for the rotational nucleus ^{164}Er is shown in fig. 3. It is nearly parabolic as expected from the I(I + 1)

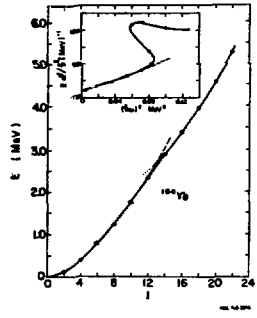

Fig. 3. Plot of excitation energy vs spin for the rotational levels of ^{164}Yb. The insert is the typical backbending plot [$2\mathcal{J}/\hbar^2$ vs $(\hbar\omega)^2$] of the same data. The dotted and dashed lines show the extensions of the two bands that cross to form the backbend.

rotational relationship, but it has a small kink around spin 14ħ. When plotted as moment of inertia, $\mathcal{J}$, versus the square of rotational frequency ħω (insert to fig. 3), this becomes a large effect. Since ħω is approximately half the γ-ray energy--directly measured--the observable effect is large. It is apparent from this insert why this is called "backbending". This anomaly was discovered by Arne Johnson and coworkers[4] in Stockholm about 10 years ago.

We now know that backbending is caused by a band crossing as shown in both the main figure and the insert of fig. 3. The ground band (pairing vacuum) is crossed by a 2-quasiparticle band. This latter band, which is lowest in energy from about 15 to 30 ħ, has been the subject of much study and is now thought to be composed of two aligned $i_{13/2}$ neutrons[5] (at least in the light rare-earth region). This concept is illustrated in fig. 4. In the usual

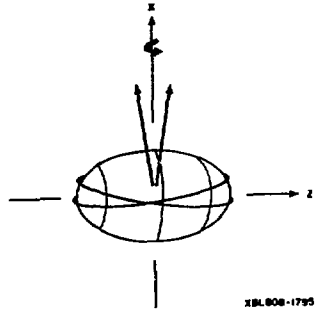

Fig. 4. Illustration of two aligned particles in a prolate nucleus with symmetry axis Z and rotation axis X.

strong-coupling scheme the particle angular momentum is coupled to the symmetry axis (Z), and its projection on that axis is called Ω. At higher rotational frequencies, the Coriolis force tends to decouple the particle angular momentum from the symmetry axis and align it with the rotation axis as shown. In this case two $i_{13/2}$ neutrons can add up to 12 $\hbar$ directly to the collective rotational angular momentum. The orbits of such aligned particles are seen (fig. 4) to be in the rotation plane and cause a triaxial bulge in the otherwise prolate nucleus. This implies that the nucleus is moving in the direction of an oblate shape rotating around the symmetry axis (60°, fig. 2), i.e. into the classically favored region of shapes as discussed above. This particular mixture of collective rotation and noncollective particle alignment turns out to be the most efficient way for the nucleus to carry angular momentum in this spin range.

That the alignment process continues at higher spins is suggested by the data shown in fig. 5. This is a backbending plot for ^{158}Er as measured by I.Y. Lee and others[6]) at Berkeley. The first backbend is much like that for ^{164}Er discussed previously, but a second irregularity occurs at frequency 0.4 MeV (around spin 28 $\hbar$). This second "backbend" has now been seen in three or four cases and shown, both experimentally and theoretically, to be due most likely to $h_{11/2}$ protons. Thus beyond spin about 30 $\hbar$, there are four aligned nucleons.

There is one more point to be made in this backbending region before going on to higher spins. The detailed work on bands in ^{160}Yb and ^{161}Yb by Lee Riedinger and others[7]) in Copenhagen is shown in fig. 6. This is a backbending plot, and the first and second backbends in the yrast sequence are very much like those discussed above. However, three side bands in ^{160}Yb and two bands in ^{161}Yb are also shown, and seem to backbend (or at least upbend) at similar frequencies ($\hbar\omega \approx 0.35$ MeV). The common feature of these five bands is that they all have one $i_{13/2}$ neutron. The 2-quasiparticle side bands in ^{160}Yb have, in addition, one other quasiparticle. The presence of a single aligned $i_{13/2}$ neutron prevents the first backbend, since one of the $i_{13/2}$ neutrons is <u>already</u> aligned, and no large backbend like that of the yrast sequence is seen in these bands. However, at somewhat higher frequencies, the <u>next best</u> $i_{13/2}$ pair can align and does so, causing the upbend observed. The important concept here is that a

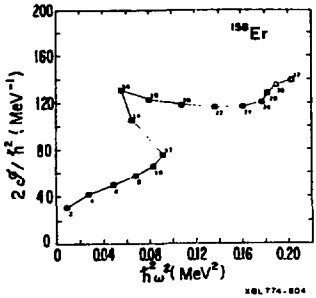

Fig. 5. Backbending plot for ^{158}Er showing the first backbend at $(\hbar\omega)^2 \approx 0.08$ and the second backbend (upbend) at $(\hbar\omega)^2 \approx 0.18$.

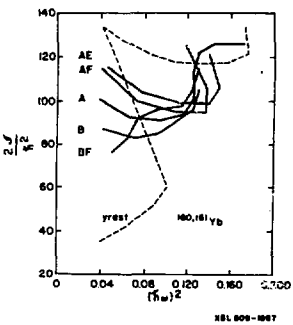

Fig. 6. Backbending plot showing the yrast sequence and three sidebands in ^{160}Yb and two bands in ^{161}Yb.

given pair of nucleons (second best $i_{13/2}$ neutron pair in this case) unpairs at a given frequency, and this happens to a large extent indpendent of the rest of the configuration. We are fortunate that the critical variable, frequency, is just half the γ-ray energy which is directly measurable. Thus, in this example, we can look for effects of the "blocked" $i_{13/2}$ backbend at a γ-ray energy of about 0.72 MeV. This concept is important for the very high-spin regions.

To summarize the situation in the backbend region, fig. 7 shows the observed bands in ^{160}Yb. The observed yrast sequence is composed of three sections having 0-, 2-, and 4-quasiparticles, respectively, as the spin increases. Above this there are many sidebands crossing one another in a seemingly complex pattern that contains much information. I could go much deeper into the details of this "backbending spectroscopy", but I want now to go on to the higher spin region.

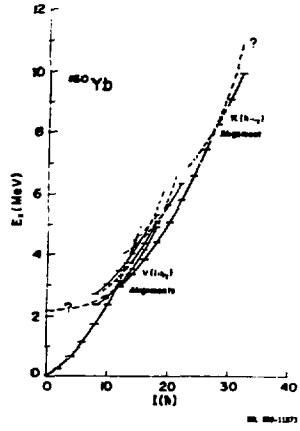

Fig. 7. Rotational band trajectories on an E vs I plot for the levels of ^{160}Yb. The observed levels are indicated by the horizontal marks.

3. Continuum region

The problem at higher spins is that the γ rays are not resolved. This is illustrated in fig. 8, where some typical γ-ray

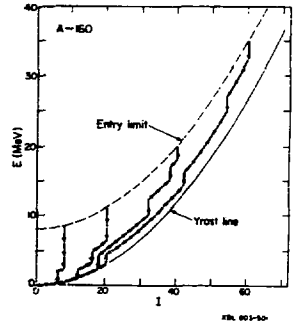

Fig. 8. Typical γ-ray deexcitation pathways to the ground state following heavy-ion fusion reactions. The statistical transitions are the vertical arrows which lower the temperature of the sytem, whereas the yrast-like transitions are roughly parallel to the yrast line and remove the angular momentum of the system.

deexcitation paths following particle evaporation are shown. Below about 20 or 30 ħ all the paths collect on or near the yrast line giving rise to intense individual γ rays that stand up in the spectrum. All the work discussed above has to do with these resolved lines. Above this spin the population is spread over hundreds or thousands of paths and no individual γ rays stand up in the spectrum. The challenge is to extract nuclear structure information without resolving this spectrum. One point illustrated

in fig. 8 is already clear. The spectrum has two components--statistical transitions that carry off the excitation energy but not much angular momentum (vertical in fig. 8) and "yrast-like" transitions that are roughly parallel to the yrast line and remove the angular momentum of the system.

An example of such a "continuum" spectrum is shown in fig. 9.

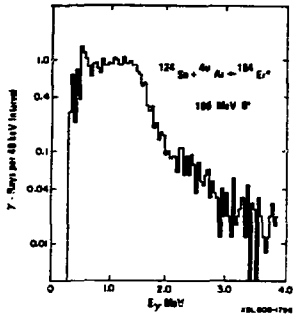

Fig. 9. Unresolved γ-ray spectrum for the indicated reaction taken with a NaI crystal and corrected for response function. The spectrum is that in coincidence with a slice of high energy (implying high spin) recorded in a large total-energy γ-ray detector.

This is a NaI spectrum, corrected for response function, so that it should represent the primary photon distribution. This particular spectrum was taken in coincidence with a 4π NaI sum crystal and corresponds to a rather broad distribution of spins whose average is about 55 $\hbar$. The details of this experimental arrangement are not important here. The final nuclei produced in this reaction are all good rotors, and it is clear that the bump below about 1.7 MeV consists of rotational transitions: they are all stretched ($I \rightarrow I - 2$) E2 transitions; the upper "edge" is correlated with the spin input in the way expected for a rotor; and the structure at energies up to about 1 MeV can all be identified with known transitions and backbends in ^{160}Er, the principal product nucleus. The exponential decrease at higher γ-ray energies is part of the statistical spectrum and not so important for nuclear structure information. Many kinds of measurements have been made on these unresolved spectra. I want to discuss here only one type--the γ-ray energy correlations. This is because my time is very limited and I believe these studies give the best insight into the physics involved in the very high spin states.

The rotor spectrum is a very simple and highly correlated one. In fig. 10 the $I(I + 1)$ energy spectrum of a rotor and the corresponding γ-ray spectrum are shown. The γ-ray spectrum consists of equally spaced lines running up to some maximum energy which is determined by the maximum spin. An example of a correlation in this spectrum is simply that no two γ rays have the same energy.

The kind of rotational correlations we are looking for are shown in greater detail in fig. 11. This is a two-dimensional display of γ-γ coincidences, with the energy of one detector plotted vertically and the other horizontally. The dots locate the coincidences from a rotational cascade having spins 2-14 $\hbar$ and a fixed moment of inertia. The absence of points along the diagonal just reflects the absence of two transitions of the same energy.

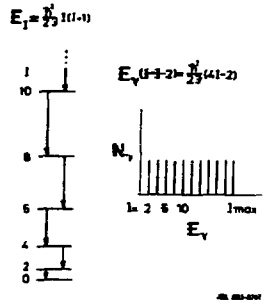

Fig. 10. The energy levels of a rotor on the left and the corresponding γ-ray spectrum on the right. Each vertical line on this spectrum represents a transition between adjacent rotational levels.

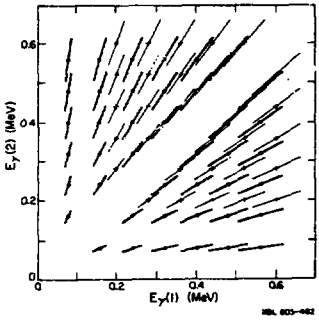

Fig. 11. Schematic correlation plot for a rotational nucleus. The dots locate the coincidences for a band with spins up to 14 ħ and moment of inertia $\mathcal{J}$, and the heavy lines show the effect of bands where $\mathcal{J}$ differs by ±10 percent. The crosses show the location of coincidences in a band with spins 16 to 26 ħ, 11 ħ of aligned angular momentum, and moment of inertia $\mathcal{J}$. The light lines again show the effect of bands differing in $\mathcal{J}$ by 10 percent.

A spread in moment of inertia by ±10% covers the range given by the lines through the dots. If an alignment of 11 ħ is assumed (reasonable for two $i_{13/2}$ neutrons), then the coincidences between states with spins 16-24 ħ and the same moment of inertia are located by the crosses. Again a ±10% spread in moment of inertia produces a spread given by the lines through the crosses. The overall pattern expected is quite clear--a valley along the diagonal and a ridge structure parallel to this valley, washing out at larger distances from the valley. Neither a spread in moment of inertia nor large alignment effects should destroy these features. The question is whether nuclei look like this at the highest spins.

An energy correlation[8,9]) spectrum from the system $^{40}Ar + ^{124}Sn$ is shown in fig. 12. A background of uncorrelated events has been subtracted from this matrix, so that one is looking at differences from the average coincidence probability. The darker areas of fig. 12 represent higher than average coincidence probability. Three features are apparent in fig. 12: there is a valley up to at least around 1.1 MeV (40 ħ), with a definite width that may become larger at higher spins; the valley is filled in places, producing "bridges"; and the valley is shallow, from 1.1 to 1.3

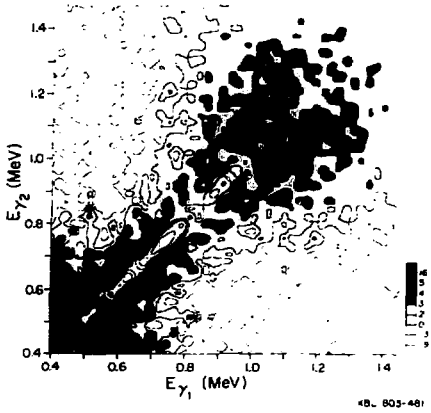

Fig. 12. Correlation spectrum from the reaction $^{124}Sn(^{40}Ar,xn)^{164-x}Er$ at 185 MeV. The data were taken on GeLi detectors and treated according to ref. 8). The plot shows contours of equal numbers of correlated events, where the darker regions have more counts according to the scale at the right edge.

MeV, and perhaps disappears altogether. There is now some understanding as to how all these features may be produced, which I want to discuss, beginning with the valley width.

The expression for rotational energy in a nucleus with some aligned angular momentum is given by

$$E = \frac{\hbar^2}{2\mathcal{J}} R(R + 1) + E_j = \frac{\hbar^2}{2\mathcal{J}} (I - j_x)^2 + E_j \quad , \qquad (1)$$

where $R = I - j_x$ is the collective angular momentum, E_j is a band head energy, j_x is the aligned particle angular momentum, and one is neglected compared with $I - j_x$. This is the equation for a parabola on an E vs I plot, which is displaced vertically (in E) by E_j and horizontally (in I) by j_x. Fig. 13 shows a series of

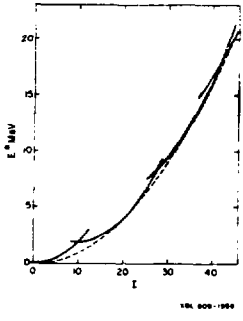

Fig. 13. Schematic illustration of the bands in a decay pathway as given by eq. (1) (solid lines) and their envelope (dashed line). The plot parameters are somewhat arbitrary but were taken to be $2\mathcal{J}/\hbar^2 = 50$ MeV^{-1} and $j_x = 0$, 10, 18, and 24 $\hbar$ for the bands, in order of increasing energy.

such parabolas with increasing E_j and j_x, and the similarity to the data of fig. 7 is unmistakable. The γ-ray energy is then given by

$$E_\gamma = 2\frac{dE}{dI} \approx \frac{\hbar}{2\mathfrak{J}} 4(I - j_x) \equiv \frac{\hbar^2}{2\mathfrak{J}_{eff}} 4I \qquad (2)$$

where we have taken j_x to be constant (for simplicity here, but probably often a reasonably good assumption), and $\mathfrak{J}_{eff}$ is defined by this relation. Generally one does not know j_x and just evaluates a moment of inertia from E_γ and I according to eq. (2), giving $\mathfrak{J}_{eff}$. To understand what $\mathfrak{J}_{eff}$ is, we note that it assumes $j_x = 0$, so that there is no horizontal displacement in fig. 13. Yet it has the same average slope as the displaced parabolas, so that it must correspond to the envelope curve (dashed in fig. 13). It is this $\mathfrak{J}_{eff}$ that should be connected with the rigid body behavior discussed in connection with fig. 2. However, the width of the valley in fig. 13 is related to the difference in γ-ray energies, given by

$$\Delta E_\gamma = 4\frac{d^2E}{dI^2} = 2\frac{dE_\gamma}{dI} = 8\frac{\hbar^2}{2\mathfrak{J}} \quad . \qquad (3)$$

The width of the valley is seen here to be related to the curvature of the parabolas, and its evaluation gives $\mathfrak{J}$, the true band moment of inertia. If the valley (in fig. 12) gets wider at higher spins it implies a smaller $\mathfrak{J}$, which, together with a large and constant $\mathfrak{J}_{eff}$ (known from other experiments), indicates larger aligned particle angular momentum, j_x. Thus, we now recognize and can measure two different moments of inertia, but the data do not yet give very reliable values for them.

In the correlation plot of fig. 12, the valley is filled at several points, the lowest two of which are around 0.6 and 0.6 MeV. These are the locations of the first and second backbends in ^{160}Er; and, indeed, backbends imply irregularities that can, and usually do, result in two or more transitions of similar energies. It seems rather clear in fig. 12 that this process continues at higher energies (spins) and may cause the general filling of the valley around 1.1-1.3 Mev. Thus we must understand the effects that alignment can produce in the correlation plot, just as we previously understood what to expect from rotational behavior.

The light lines in fig. 14 trace out the trajectory of two perfect rotational bands in the spin versus frequency plane. The dots along these lines indicate the actual γ-ray transitions. The steeper line corresponds to a rigid-sphere moment of inertia, whereas the other line has about half that value. This latter value for moment of inertia is probably more realistic over the entire spin range; at low spins due to pairing effects and at higher spins due to single particle alignments as discussed above. Note that the frequency range 0-0.8 MeV corresponds to γ-ray energies 0-1.6 MeV, the observed range (see fig. 9). The vertical lines in fig. 14 mark the frequencies where the important aligned high-j orbitals approach the Fermi level as given by recent calculations[10]. The neutron $i_{13/2}$ ($\hbar\omega$ = 0.25 MeV) and the proton $h_{11/2}$ ($\hbar$ = 0.45 MeV) orbitals cause the first and second backbends observed in the yrast cascade as discussed above. The concept discussed in connection with fig. 6 now becomes important: at these critical frequencies the indicated aligned orbital will be populated (with increasing spin, or depopulated with decreasing spin) in essentially all bands (except where blocking occurs) irrespective of the rest of the configuration. We do not really

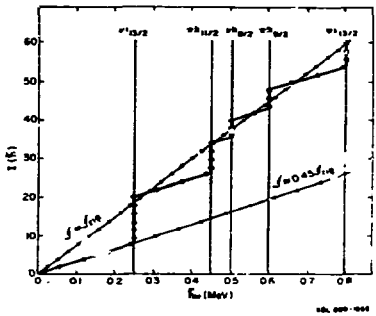

Fig. 14. Plot of spin vs rotational frequency ($E_\gamma/2$). The light lines show the trajectories of rotors having moments of inertia equal to (above) and 0.45 times (below) the rigid-body value. The vertical lines indicate the frequencies where the important high-j orbitals come near the Fermi level. The heavy line represents a trajectory for a realistic nucleus involving both rotation and alignment.

know how narrow the frequency range for each orbital will be, but fig. 6 gives some hope that it will be reasonably narrow. Thus the trajectory in fig. 14 followed by a real nucleus would be something like the heavy line. The frequency increases with rotation until one of the critical frequencies is reached. Then the angular momentum of that aligned particle(s) is exhausted, after which the frequency again increases with spin. Each alignment is drawn as an upbend in fig. 14, whereas a backbend results if the nucleus remains on the rotational trajectory beyond the critical frequency and then jumps back suddenly to the more aligned band at some higher spin value. Note that relating spin and frequency (γ-ray energy) places one (on the average) on the $\mathcal{J}_{rig}$ line--$\mathcal{J}_{eff} = I/\omega \rightarrow \mathcal{J}_{rig}$. On the other hand, the valley width results from two successive rotational transitions, which relates to the slope of the rotational segments in fig. 14--$\mathcal{J} = dI/d\omega \rightarrow 0.45\,\mathcal{J}_{rig}$. Thus we see pictorially examples of the two moments of inertia discussed above. Note, however, that rather few transitions fall on the rotational segments after the second backbend region ($\hbar\omega \gtrsim 0.45$). A point on the first ridge of a correlation plot requires two adjacent transitions along a rotational segment, and we see that this is not so common in fig. 14 at higher frequencies--in spite of the fact that there are not really many important orbital alignments (five total). We can thus understand why the valley might wash out at higher spins in fig. 12.

To see more clearly the implications of alignment, I have plotted in fig. 15 the coincidences resulting from adjacent transitions in fig. 14. This figure is plotted from $E_\gamma = 0.4$-1.7 MeV, much as fig. 12. One sees collections of points along the valley corresponding to the alignments, and the first ridge is reasonably well outlined (dashed line). Inclusion of nonadjacent transitions would put some additional points in the valley and fill out the more distant ridges--they would not contribute further to the first ridge. One feature that is apparent is that there must be enhanced rows and columns through the bridges--as indicated by the light lines in fig. 15. The occurrence of two or more transitions at these energies will cause additional coincidences all along that row and column. Unfortunately, the mathematical procedure for subtracting uncorrelated events suppresses observation of these enhanced rows and columns; in correlated spectra like fig. 12 each row and column must sum to zero. A new iteration technique has

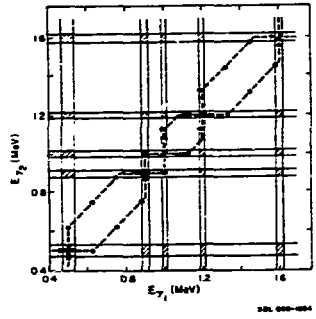

Fig. 15. The correlation-type spectrum generated by considering only the adjacent transitions in fig. 14. The light lines indicate the locations where more intense rows and columns will be found.

been invented very recently by Bent Herskind to correct (in part) this problem; and, while we still do not understand this technique very well, I cannot resist showing you a spectrum processed this new way.

The data in fig. 16 are from the reaction ^{130}Te + ^{40}Ar (185 MeV), and have been processed by the iterative technique[11]. The

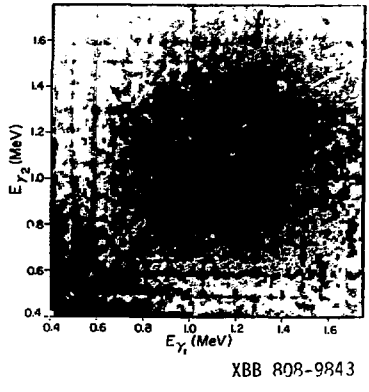

Fig. 16. The correlation-type spectrum from the reacton ^{130}Te + ^{40}Ar treated by the new iterative procedure.

pattern of enhanced rows and columns is clear. The first backbend in the 0.4-0.6 MeV region is extremely strong, and the second at nearly 0.9 MeV is also well defined. Most surprising, perhaps, is the very strong feature at 1.3 MeV, which surely corresponds to spins around 50 $\hbar$. Even the row and column at nearly 1.6 MeV (~60 $\hbar$) is quite clear. Overall, this pattern looks very much like that

expected (fig. 15), even to the extent that the number of strong features (~5) corresponds very roughly to the number of important high-j orbitals. Remember that the spread in frequencies from a given orbital might be rather large and that blocking effects might produce weaker features at different frequencies (like the blocked first backbend known to be at ~0.73 MeV).

It should be clear, however, that we do not yet understand these iterated spectra very well. The observed rows and columns are weak features--surely no more than 5-10% of the full population through the appropriate spin region--and they are surprisingly narrow, 15-20 keV wide at times. Although they are not simple statistical variations, their detailed structure is very sensitive to the details of selection--sum crystal slice, multiplicity fold, etc. There is much yet to be learned about these spectra, but they surely seem very exciting and promising at the present time.

4. Conclusion

The correlation technique just described implies that there may be special frequencies (γ-ray energies) in nuclei which might be used to select events corresponding to a given γ-decay pathway. I want to conclude by mentioning another new method for selecting events. These are 4π spherical shells of NaI that absorb essentially all the γ rays emitted in the decay of a product nucleus (like a sum crystal) and, in addition, are divided into many segments to determine the number and energies of individual γ rays. Such "multiplicity detectors" are being built at present in Oak Ridge (70 segments) and G.S.I. Darmstadt (160 segments). A photograph of the Oak Ridge instrument being constructed by Demetrius Sarantites is shown in fig. 17. These instruments will determine multiplicity (spin) to about 20% and also total γ-ray energy to about the same precision. Referring to fig. 8, this corresponds to a selection of entry conditions in both dimensions plotted, energy and spin. It is hard to imagine what we will learn from studying the γ decay from such small population regions.

This area of very high spins seems to me at present to be very active and promising. There is real hope for understanding some details of nuclear structure at 60 ħ in the next few years.

Fig. 17. A photograph of the 4π multiplicity detector recently constructed at Oak Ridge National Laboratory.

XBB 809-10872

References

1) A. Bohr and B.R. Mottelson, Nuclear Structure, vol. 2 (Benjamin, Reading, Mass, 1975)

2) T.L. Khoo, R.K. Smither, B. Haas, O. Hausser, H.R. Andrews, D. Horn, D. Ward, Phys. Rev. Lett. 41 (1978) 1027

3) O. Hausser, H.-E. Mahnke, J.F. Sharpey-Schafer, M.L. Swanson, P. Taras, D. Ward, R.R. Andrews, T.K. Alexander, Phys. Rev. Lett. 44 (1980) 132

4) A. Johnson, H. Ryde, J. Sztarkier, Phys. Lett. 34B (1971) 605

5) F.S. Stephens and R.S. Simon, Nucl. Phys. A183 (1972) 257

6) I.Y. Lee, M.M. Aleonard, M.A. Deleplanque, Y. El Masri, J.O. Newton, R.S. Simon, R.M. Diamond, F.S. Stephens, Phys. Rev. Lett. 38 (1977) 1454

7) L.L. Riedinger, O. Andersen, S. Frauendorf, J.D. Garrett, J.J. Gaardhøje, G.B. Hagemann, B. Herskind, Y.V. Makovetsky, J.C. Waddington, M. Guttormsen, P.O. Tjøm, Phys. Rev. Lett. 44 (1980) 568

8) O. Andersen, J.D. Garrett, G.B. Hagemann, B. Herskind, D.L. Hills, L.L. Riedinger, Phys. Rev. Lett. 43 (1979) 687

9) M.A. Deleplanque, F.S. Stephens, O. Andersen, C. Ellegaard, J.D. Garrett, B. Herskind, D. Fossan, M. Neiman, C. Rouvet, D.C. Hillis, H. Kluge, R.M. Diamond, R.S. Simon, Phys. Rev. Lett. 45 (1980) 172

10) S. Frauendorf, private communication (1980)

11) C. Ellegaard, M.A. Deleplanque, O. Andersen, J.D. Garrett, B. Herskind, R.M. Diamond, H. Kluge, M. Neiman, C. Schuck, S. Shih, and F.S. Stephens, unpublished data 1980

This work was supported by the Division of Nuclear Physics of the Office of High Energy and Nuclear Physics of the U.S. Department of Energy under Contract W-7405-ENG-48.